Comparison of two multifunctional catalysts [M/Nb_2O_5 (M = Pd, Pt)] for one-pot hydrodeoxygenation of lignin

Lin Dong, Yi Shao, Xue Han, Xiaohui Liu, Qineng Xia, Stewart F. Parker, Yongqiang Cheng, Luke L. Daemen, Anibal J. Ramirez-Cuesta, Yanqin Wang and Sihai Yang

Published version information

Citation: L Dong et al. "Comparison of two multifunctional catalysts [M/Nb_2O_5 (M = Pd, Pt))] for one-pot hydrodeoxygenation of lignin." Catalysis Science & Technology, vol. 8, no. 23 (2018): 6129-6136.

DOI: 10.1039/c8cy01459k

Comparison of Two Multifunctional Catalysts [M/Nb_2O_5 (M=Pd, Pt)] for One-Pot Hydrodeoxygenation of Lignin

Lin Dong,[δa] Yi Shao,[δa] Xue Han,[b] Xiaohui Liu,[a] Qineng Xia,*[c] Stewart F. Parker,[d] Yongqiang Cheng,[e] Luke L. Daemen,[e] Anibal J. Ramirez-Cuesta,[e] Yanqin Wang*[a] and Sihai Yang*[b]

Improved lignin valorisation *via* its catalytic conversion to value-added feedstocks is of essential importance to the development of future bio-refineries. The identification of active binding domains within a catalyst structure provides important insights into the function of catalysts. Vibrational analysis employing inelastic neutron scattering (INS) enables the full interrogation of the dynamics of hydrogen in host-guest systems. Here we report an *in situ* INS investigation of the catalytic origins of two multifunctional catalysts [M/Nb_2O_5 (M=Pd, Pt)] for the hydrodeoxygenation (HDO) of phenol, a key model compound for lignin. We also report the excellent activity of these two catalysts for the conversion of raw lignin into hydrocarbons showing (i) complete removal of the oxygen content; (ii) near-quantitative yields of C_7-C_9 products based upon lignin monomers and (iii) different reaction networks. The *in situ* INS study has revealed the molecular details directly underpinning their distinct reaction pathways. We found that on the Pd/Nb_2O_5 catalyst, the hydrogenation of phenyl rings has higher selectivity than the direct cleavage of C–O bonds owing to the strong binding of the phenyl ring to the catalyst surface and high hydrogenation activity of Pd, while on the Pt/Nb_2O_5 catalyst, the HDO reaction undergoes a combination of direct dehydroxylation (DDO) process and tandem route with fast kinetics, leading to a higher selectivity of arene than that of Pd/Nb_2O_5 at the beginning of the reaction.

1 Introduction

Hydrogenation occurs and dominates many chemical and biological processes. In the field of catalysis, the behavior of hydrogen is often the primary concern that governs the product selectivity.[1] However, operando characterisation of hydrogen atoms involved in catalytic reactions is extremely challenging, not least because of their invisibility in X-ray scattering experiments and low sensitivity in optical spectroscopic measurements. Inelastic neutron scattering (INS) is a powerful neutron spectroscopy technique to investigate the dynamics of hydrogenous compounds by exploiting the ultra-high neutron scattering cross-section of hydrogen, which is almost an order of magnitude higher than all other elements.[2] Additionally, INS is not subject to any optical selection rules and can readily access the low energy modes (< 500 cm^{-1}), and thus is well suited to study the deformational and conformational dynamics of the catalyst-substrate system.

Catalytic conversion of renewable biomass to value-added feedstocks *via* hydrodeoxygenation (HDO) reactions is increasingly recognised as a sustainable pathway to bridge the future gaps in the supply of fuels and chemicals.[3] Among the three components (*i.e.*, cellulose, hemicellulose and lignin) in lignocellulosic biomass, lignin, consisting of a heterogeneous and irregular aromatic biopolymer, is most challenging to chemical transformation. Current research is centered at developing efficient strategies for the depolymerisation of lignin network to a wide spectrum of phenolic monomers[4] and the subsequent hydrogenolysis of the low-molecular-weight lignin monomers into fuels or feedstocks.[5] In our earlier work, a Ru/Nb_2O_5 catalyst was developed for the conversion of raw lignin to hydrocarbons with both high yields and arene selectivities.[5c] Phenol or substituted phenols are often used as model compounds to evaluate the HDO activity of a given catalyst or catalytic system.[6] To date, three types of reaction mechanisms have been proposed for the HDO of phenol primarily based upon the analysis of product distribution during the reaction. The first one is the tandem reaction over bifunctional catalysts, where phenol is initially hydrogenated to cyclohexanol, or cyclohexanone through a keto-tautomer intermediate route on metal sites, followed by dehydration on the acid support to form cyclohexene, and then dehydrogenated to benzene[7] or further hydrogenated to cyclohexane.[8] An alternative route is the dehydroxylation mechanism, in which the C–O bond in phenol is directly cleaved with benzene as the main product.[9] The third way was proposed for the conversion of *m*-cresol on the NiFe bimetallic catalyst[10] and Pt/SiO_2 catalyst,[11] where adsorbed phenolic compounds firstly undergo a keto−enol tautomerisation reaction[12] followed by carbonyl hydrogenation to cyclohexadienol and then dehydration to form aromatic products. DFT modelling has been widely used to provide theoretical insights into these HDO mechanisms of phenol on Pd,

[a]:*Shanghai Key Laboratory of Functional Materials Chemistry, Research Institute of Industrial Catalysis, School of Chemistry and Molecular Engineering, East China University of Science and Technology, Shanghai, 200237, P. R. China. Email: wangyanqin@ecust.edu.cn*
[b]: *School of Chemistry, University of Manchester, Manchester, M13 9PL, UK. Email: Sihai.Yang@manchester.ac.uk*
[c]:*School of Biology and Chemical Engineering, Jiaxing University, Zhejiang 314001, PR China. Email: qinengxia159@163.com*
[d]: *ISIS Facility, STFC Rutherford Appleton Laboratory, Chilton, Oxfordshire, OX11 0QX, UK.*
[e]: *The Chemical and Engineering Materials Division (CEMD), Neutron Sciences Directorate, Oak Ridge National Laboratory, Oak Ridge, TN 37831, USA.*
[δ]: *These two authors contribute equally.*
† Electronic Supplementary Information (ESI) available. See DOI: 10.1039/x0xx00000x

Pt, Ru and Fe catalysts.[12] However, experimental evidence to support the stepwise reaction network is largely lacking and little effort has been devoted to identifying the catalyst-substrate binding interactions. Recently, there are emerging studies on catalytic reactions by INS;[13] however, its use for investigations on biomass conversion is rarely reported.[5c,14] Here we report the catalytic conversion of raw lignin to hydrocarbons with exceptionally high yields *via* HDO reactions over the M/Nb_2O_5 (M = Pd, Pt; M loading at 2 wt%) catalysts. Pd and Pt, as the most conventional HDO catalysts, are selected for investigation in this study. More importantly, we report a detailed vibrational analysis *via in situ* INS on the adsorption, binding and reaction mechanisms of phenol over the catalyst surface, where two distinct reaction pathways have been revealed by experiments.

2 Experimental

2.1 Materials

The chemicals were purchased from commercial suppliers and used as provided: 4-methylphenol (J&K Chemical, 99%), phenol (J&K Chemical, 99%), propylbenzene (TCI, >99% GC assay), ethylbenzene (TCI, >99% GC assay), 4-methylcyclohexanol (TCI, >98% GC assay), 4-methylcyclohexanone (TCI, >98% GC assay), methylcyclohexane (Macklin, ≥99.8% GC assay), ethylcyclohexane (J&K Chemical, 99%), propylcyclohexane (TCI, >98% GC assay). $Pd(NO_3)_2$ and $Pt(NO_3)_2$ solutions were purchased from Heraeus Materials Technology Shanghai Co., Ltd. Birch wood was purchased from local manufactory (*ca.* 40 mesh), and dried at 100 °C for 5 h before use. All other chemicals were purchased from Sinopharm Chemical Reagent Co., Ltd. and used without purification.

2.2 Lignin extraction and isolation

Birch lignin was extracted according to a literature procedure.[15] In a 1 L round-bottom flask with condenser, 40 g of pre-ground birch wood and 400 mL methanol containing 3% hydrogen chloride by weight were combined. The mixture was refluxed for 12h under stirring, and cooled to room temperature. Residue was removed by suction filtration and washed with additional small portions of methanol. The filtrate was concentrated to < 200 mL by rotary evaporation then poured into 1 L of ice-cold water with vigorous stirring, causing a light brown solid to precipitate. This lignin was collected by filtration, washed with a small portion of water and dried under vacuum. The yield of dried, crude birch lignin was 4.97 g (12.4 wt%). The Gel Permeation Chromatography (GPC, Waters 1515) was performed to analyse the molecular weights of the extracted lignin. Before analysis, lignin was dissolved in THF. A calibration curve was obtained using monodisperse polystyrene standards. The result was shown in Table S1.

2.3 Catalyst preparation

Nb_2O_5 was synthesised according to published procedures.[16] The Pd- and Pt-based catalysts were prepared by the incipient wetness impregnation method with appropriate amounts of aqueous solution of $Pd(NO_3)_2$ and $Pt(NO_3)_2$, respectively. The obtained sample was dried at 100 °C for 12h and then calcined at 500 °C for 3h (heating rate 1 K min^{-1}). Before reaction, Pd- and Pt-based catalysts were reduced in a 10% H_2/Ar flow at 400 °C for 3h. The metal loading in each catalyst was at 2 wt%.

2.4 Characterisation

Powder X-ray diffraction (PXRD) patterns were recorded on a Rigaku D/max-2550VB/PC using Cu Kα radiation (λ = 1.5406 Å). Transmission electron microscopy (TEM) images were recorded on a FEI Tecnai F20 s-TWIN instrument, and the electron beam accelerating voltage was at 200 kV. Nitrogen adsorption experiments were performed at 77 K on Micromeritics ASAP 2020 M sorption analyzer. The BET method was used to calculate the specific surface area.

2.5 Catalytic test and product analysis

The detailed reaction conditions are described in the figure captions and table footnotes. In a typical reaction, catalyst (0.2 g) and lignin (0.1 g) were loaded into a stainless-steel autoclave reactor (Anhui Kemi Machinery Technology Co., Ltd) with water (15 mL) as the solvent. After the reactor was purged with H_2 three times and charged with 0.7 MPa H_2, the reaction was conducted at 250 °C with a magnetic stirring speed of 600 rpm. After the reaction, the reactor was quenched to ambient temperature in an ice-water bath, and the organic products were extracted using ethyl acetate and analysed by gas chromatography (GC) and GC-mass spectroscopy (GC-MS) on an Agilent 7890B gas chromatograph with flame ionisation detector (FID) and an Agilent 7890A GC-MS instrument, both equipped with HP-5 capillary columns (30 m × 250 μm). Tridecane was used as an internal standard for the quantification of the liquid products.

2.6 *In situ* inelastic neutron scattering (INS)

INS spectra were recorded on the TOSCA spectrometer at the ISIS Facility at the STFC Rutherford Appleton Laboratory (UK) and on the VISION spectrometer at Spallation Neutron Source, Oak Ridge National Laboratory (USA). Both TOSCA and VISION are indirect geometry crystal analyser instruments that provide a wide dynamic range (16–4000 cm^{-1}) with resolution optimised in the 50–2000 cm^{-1} range. In this region TOSCA has a resolution of 1.25% of the energy transfer. All the INS spectra for the catalysis system were collected after the sample was cooled and stabilised at temperatures below 30 K.

Approximately 20 g of each catalyst was loaded into a flow type stainless steel cell. By heating at 300 °C under He flow for 3 hours, the trace amount of water that was adsorbed on the catalyst surface was removed. The activated catalyst was then

reduced by heating under H_2 flow at 150 °C for 3 h. To study the reaction mechanism, phenol was used as a model compound and dosed into the sample cell by a He flow at 150 °C for 3 h. This allowed phenol to be adsorbed on the catalyst surface and the INS spectrum of the phenol adsorbed catalyst was collected after cooling to below 30 K. After the data collection, phenol/H_2 was introduced to the cell for 7 min at 150 °C for the catalytic reaction to occur. The exhaust gas was monitored continuously *via* mass spectrometry.

Table 1. Summary of product yields from direct hydrodeoxygenation of birch lignin.[a]

	Products distribution (wt%/)									RMY[e] (%)	Total mass Yield (wt%)/(C%)
	C_7~C_9 arenes			C_7~C_9 cycloalkanes							
Catalyst	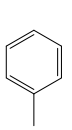	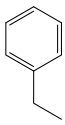	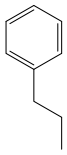	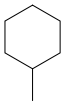	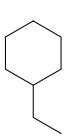	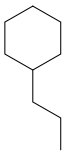	Other C_7~C_9[b]	C_{10}~C_{15}[c]	Others[d]		
Pd/Nb_2O_5	0.2	0.4	1.7	3.3	7.4	10.4	1.7	3.7	3.1	73.7	31.9/42.2
Pt/Nb_2O_5	0.2	1.5	2.1	1.8	10.4	11.2	1.0	3.0	3.5	85.2	34.7/46.1

[a] Reaction conditions: lignin 0.1 g, catalyst 0.2 g, H_2O 15 mL, 250 °C, H_2 0.7 MPa, 20h, stirring at 1000 rpm. The metal loading in each catalyst was at 2 wt%.

b 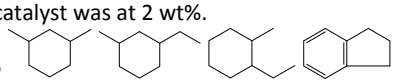

c 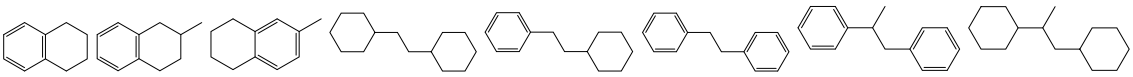

[d] C_{16} and C_{17} aliphatic alkanes and other products were only quantified by GC but not confirmed for structures.

[e] Ratio of molar yields (RMY) = (total yield of monocyclic compounds) / (theoretical yield of monocyclic compounds from NBO) ×100%. Theoretical yield of monocyclic compounds from birch lignin is 2741 μmol g^{-1}.

A further reaction was carried out by feeding H_2 for an additional 0.5-2 hours at 150 °C. INS spectra of pure solid compounds for both starting material and reaction products were collected at 10 K. DFT calculations of the INS spectra for solid compounds were carried out. The information was used to identify the modes of vibrational features in the experimental INS spectra. A detailed description of DFT calculations is given in supporting information. Throughout this report, no scaling factor was used.

3 Results and Discussions

3.1 Characterization of catalysts

Mesoporous Nb_2O_5 was used as the support for Pd/Nb_2O_5 and Pt/Nb_2O_5 catalysts. Fig. S1 shows the X-ray powder diffraction patterns of mesoporous Nb_2O_5 and bulk Nb_2O_5. All diffraction peaks of the bulk phase can be indexed to the orthorhombic Nb_2O_5 (JCPDS card 300873). For mesoporous Nb_2O_5, the overall intensity of diffraction peaks is reduced with only main peaks observed, indicating that the crystallinity of mesoporous Nb_2O_5 is poor. The TEM images show that Pd and Pt particles are homogeneously distributed on the Nb_2O_5 support (Fig. S2a, S2b). The metal dispersions of Pd and Pt are determined as 24.5% and 55.0%, respectively, according to CO chemisorption. The surface area of used Pd/Nb_2O_5 and Pt/Nb_2O_5 catalyst after four runs both show a small decrease (from 82 to 69 m^2g^{-1} and from 96 to 77 m^2g^{-1}, respectively).

3.2 Catalytic HDO of raw lignin

The HDO of birch lignin was conducted at 250 °C with 0.7 MPa H_2 for 20 h over the M/Nb_2O_5 (M= Pd, Pt) catalysts in an aqueous solution. In both cases, the products are mixtures of hydrocarbons (arenes and alkanes) *via* the complete removal of oxygen functional groups from the raw lignin (Table 1). The mass yields of liquid hydrocarbons of reactions over the Pd/Nb_2O_5 and Pt/Nb_2O_5 catalysts are 31.9 wt% and 34.7 wt%, respectively, comparable to that observed over Ru/Nb_2O_5 (35.5 wt%).[5c] Considering that the oxygen content accounts for 27.9 wt% (Table S2) and removed by –OH or $–OCH_3$ functional groups, these yields obtained are exceptionally high. The main products here are cycloalkanes, and are different from the result from Ru/Nb_2O_5, where arenes are main products.[5c] The liquid products over the Pd/Nb_2O_5 catalyst is composed of 7.2 wt% C_7~C_9 arenes, 71.5 wt% C_7~C_9 cycloalkanes, and 11.6 wt% C_{10}~C_{15} dicyclic arenes and dicyclic cycloalkanes. Similarly, that over the Pt/Nb_2O_5 catalyst includes 11.0 wt% C_7~C_9 arenes, 70.3 wt% C_7~C_9 cycloalkanes, as well as 8.6 wt% C_{10}~C_{15} dicyclic arenes and dicyclic cycloalkanes. Significantly, the total yields of C_7~C_9

hydrocarbons on the Pd/Nb_2O_5 (25.1 wt%, 2020 μmol/g lignin) and Pt/Nb_2O_5 catalysts (28.2 wt%, 2335 μmol/g lignin) compare favorably with the theoretical yield (2741 μmol/g lignin) obtained through the nitrobenzene oxidation of raw lignin (Fig. S3a), which is an established lignin monomer analysis method. The influence of the substrate/catalyst ratio on the product distribution was also investigated (Table S4). With half amount of catalyst, the total yields of liquid hydrocarbons of reactions over the Pd/Nb_2O_5 and Pt/Nb_2O_5 decreased to 12.9 and 13.9 wt%, respectively, with a little amount of oxygen-containing products. This decreased is likely due to a reduced catalyst/lignin contact since the lignin is insoluble in water. Nonetheless, the products distribution was similar to that with 0.2g of catalyst, suggesting that the nature of the lignin/catalyst interaction remains the same regardless of the substrate/catalyst ratio. To investigate the catalytic activity of lignin from paper and pulp industry, the direct hydrodeoxygenation of alkaline lignin was also conducted in the same reaction condition (Table S5). The total yields of C_7~C_9 hydrocarbons from alkaline lignin on the Pd/Nb_2O_5 (12.1 wt%, 773 μmol/g lignin) and Pt/Nb_2O_5 catalysts (13.0 wt%, 893 μmol/g lignin) compare favorably with the theoretical yield (1040 μmol/g lignin) (Fig. S3b). Thus, both catalysts have shown excellent HDO activity for the conversion of lignin to hydrocarbons.

The stabilities of Pd/Nb_2O_5 and Pt/Nb_2O_5 catalysts for the conversion of birch lignin were tested by using substrate (0.1 g)/catalyst (0.1 g) ratio in four consecutive recycling runs (Fig. S4 and Table S3). In both cases, the activities decreased after the first run and stayed constant in the subsequent three recycling runs, indicating that the fresh catalyst is likely reconstructed, and then stabilized. The used catalysts were sequentially characterized by XRD, TEM and ICP. TEM (Fig. S2c, S2d, Fig. S5) and ICP showed a slight enlargement of nanoparticles and a small leaching of Pd/Pt. All these factors may be attributed to the decrease of the HDO activity in the cycling experiments.

3.3 Catalytic studies of model compound

To study the product distribution, the HDO of 4-methylphenol (**0**) as a model compound for lignin was investigated at 250 °C and 0.5 MPa H_2, and the time profiles plotted in Fig. 1. Over the Pd/Nb_2O_5 catalyst, the primary products at low conversion of 13.5% (t = 0.5h) consists of toluene (**1**) (***S*** = 11.2%), 4-methylcyclohexanone (**5**) (***S*** = 81.9%) and 4-methylcyclohexanol (**4**) (***S*** = 5.8%). As the reaction time prolonged (t > 2h), the selectivity to **1** reached and retained a maximum value of *ca.* 23%. In the meantime, **5** was hydrogenated to **4** and subsequently to methylcyclohexane (**2**),which is the main product (***S*** = 44.9%). In contrast, over the Pt/Nb_2O_5 catalyst, **0** was completely and rapidly converted at the beginning of reaction, affording **1** (***S*** = 37.3%) and **4** (***S*** = 31.4%) with a small amount of **2** and **5**. At 2h, as well as the rapid increase of **2**, the yield of **1** surprisingly also increased. Considering that **0** was completely converted at 1h, this result indicates that **1** was obtained from a combinatin of the DDO (direct dehydroxylation) process and the tandem reaction,[7] in which the intermediate, **4** was firstly converted to **3**, and then dehydrogenated to arenes *via* hydrogen transfer.

Furthermore, the conversion of **4** over the M/Nb_2O_5 (M = Pd, Pt) catalysts was also investigated to validate the tandemreaction pathway. As shown in Table 2, the toluene yield over the Pd/Nb_2O_5 catalyst is only 3.8% (***S*** = 9.1%), much lower than that (20.8%) over the Pt/Nb_2O_5 catalyst (***S*** = 32.6%), indicating that Pt can enable the tandem reaction, leading to the production of arenes. Interestingly, albeit the low metal loading, these two catalysts display distinct reaction pathways (Fig. 2), indicating the critical importance of hydrogen activity in this reaction.

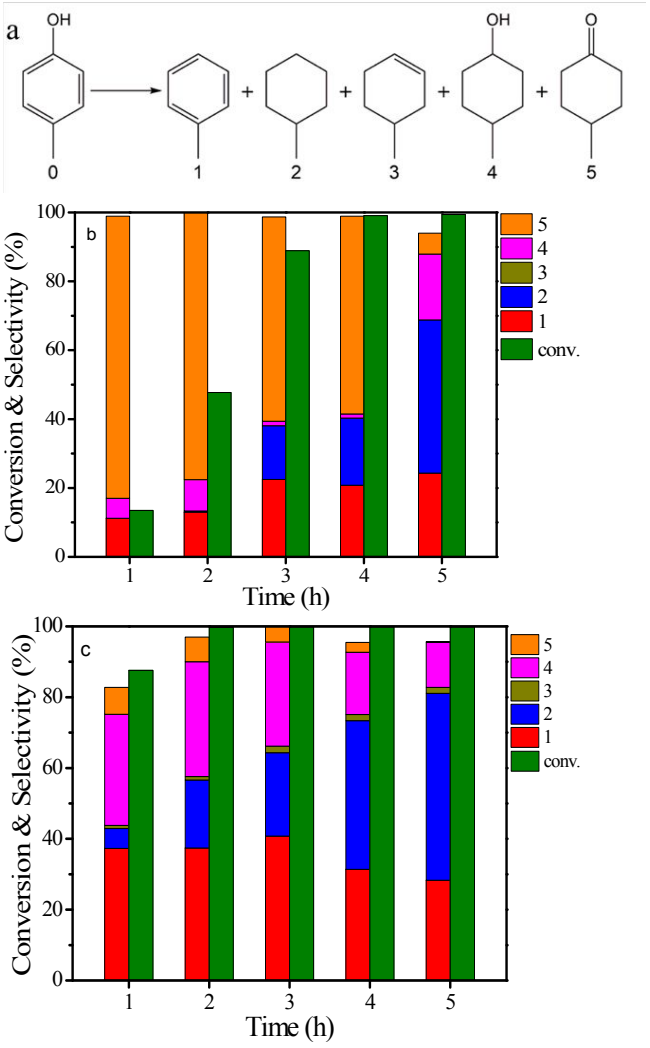

Fig. 1 (a) View of the chemical structures for all possible intermediates and products for the HDO of 4-methylphenol. Variation of the product selectivity for the conversion of 4-methylphenol over the Pd/Nb_2O_5 (b) and Pt/Nb_2O_5 (c) catalysts as a function of time. Reaction conditions: substrate 0.2 g, catalyst 0.4 g, H_2O 15 mL, 250 °C, H_2 0.5 MPa, stirring at 1000 rpm.

Table 2. Product distribution for the HDO conversion of 4-methylcyclohexanol over Pd/Nb_2O_5 and Pt/Nb_2O_5 catalysts.[a]

Catalyst	Conv. (%)	Yield/Selec.[b] (%)			
		1	2	3	5
Pd/Nb_2O_5	41.8	3.8/9.1	27.0/64.6	1.0/2.4	4.4/10.5
Pt/Nb_2O_5	63.8	20.8/32.6	26.1/40.9	0.4/0.6	8.5/13.3

[a] Reaction conditions: 4-methylcyclohexanol 0.2 g, catalyst 0.4 g, H_2O 15 mL, 250 °C, H_2 0.5 MPa, 4 h, stirring at 1000 rpm. The metal loading in each catalyst was at 2 wt%.
[b] The chemical structures of the products are shown in Fig. 1a.

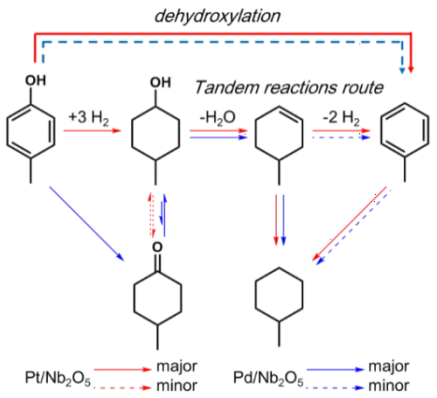

Fig. 2 Reaction pathways of the conversion of 4-methylphenol over Pt/Nb_2O_5 and Pd/Nb_2O_5 catalysts.

3.4 INS investigations on the reaction mechanisms

Direct visualisation of the dynamics of substrate molecules on the catalyst surface is crucial to understand the molecular details of binding and HDO of phenol. Here *in situ* INS has been applied to investigate the vibrational properties of phenol–M/Nb_2O_5 (M = Pd, Pt) systems to reveal the molecular origins on HDO of phenol over these two catalysts showing different reaction pathways.

Pd/Nb_2O_5 was activated and reduced by heating at 300 °C under a He flow for 3 hours, followed by a H_2 flow at 150 °C for another 3 hours. Upon reduction in H_2, the INS spectrum shows higher intensity than that of the activated catalyst, indicating the formation of hydrogenous species on the surface (Fig. S6). The new features at 489 and 966 cm^{-1} are consistent with the formation of surface Pd–H and Nb–O–H bonds. Interestingly, the vibration mode of Pd–H has been reported at ~480 cm^{-1} by an INS study.[17]

Upon phenol adsorption at 150 °C, a significant increase in total intensity and the appearance of many new spectral features were observed, clearly demonstrating the binding of phenol molecules onto the catalyst surface (Fig. S8). Difference INS spectrum of adsorbed phenol species was obtained by subtracting the INS spectrum of the reduced catalyst from the phenol adsorbed catalyst (Fig. 3a, S9). By comparing the difference spectrum and the INS spectrum of solid phenol at 10 K, a few changes were clearly observed. Peaks at low energy (below 120 cm^{-1}), assigned to the translational and rotational modes of phenol, shift to lower energy with a continuum profile, suggesting that the adsorbed phenol molecules are disordered over the catalyst surface and have restricted translational motion owing to the strong binding to the catalyst. The intensity of the peaks between 155 and 242 cm^{-1} (librational modes of adsorbed phenol molecules) was greatly decreased, consistent with the restricted motion of the C6-ring upon adsorption. The peaks at 532 and 724 cm^{-1} (assigned to the C6-ring deformation and out-of-plane wagging of –CH–, respectively) also concurrently reduced in intensity upon binding. The broad peaks at 1238 and 1378 cm^{-1} (assigned to the combination of in-plane wagging of –OH and

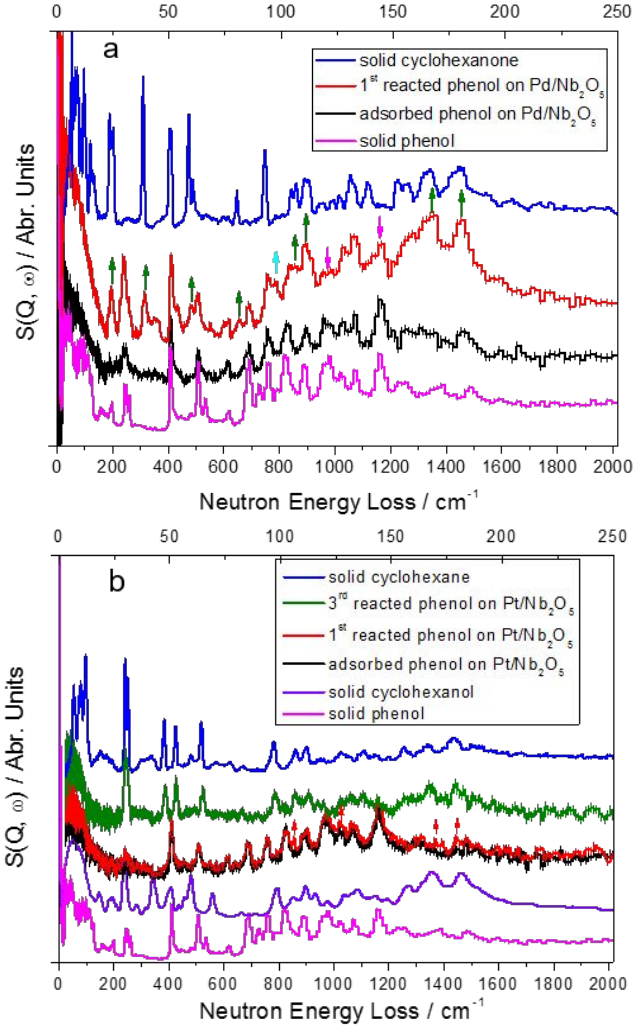

Fig. 3 INS spectra for Pd/Nb_2O_5 and Pt/Nb_2O_5 during the adsorption and catalytic HDO of phenol. INS spectrum of the reduced catalyst was used throughout for calculations of the

difference spectra. (a) Comparison of the INS spectra of the adsorbed and 1st reacted phenol on the Pd/Nb_2O_5 catalyst. (b) Comparison of the INS spectra of the adsorbed, 1st and 3rd reacted phenol on the Pt/Nb_2O_5 catalyst. The INS spectra of solid cyclohexanone, cyclohexane and phenol are shown for comparison.

in-plane rocking of –CH–) almost disappeared, suggesting the deprotonation of adsorbed phenol molecules to form phenoxide bound on the catalyst surface. Overall, the out-of-plane modes of phenol molecules are affected more significantly than the in-plane modes upon adsorption, indicating the presence of "near flat" orientations for bound molecules on the catalyst surface.

INS spectra of the reaction system were collected after an H_2/phenol stream flowing through the phenol adsorbed catalyst at 150 °C for an initial 7 minutes and a further 2 hours, the latter of which was done under a pure H_2 flow. Comparison of the INS spectra for adsorbed, 1st reacted and 2nd reacted phenol on the Pd/Nb_2O_5 catalyst show marked changes (Fig. S10). The INS spectrum of the 1st reacted system shows much enhanced intensity comparing to that of the adsorbed phenol, whereas that of the 2nd reacted phenol displays an overall much lower intensity. This observation indicates that the adsorbed phenol molecules underwent a partial hydrogenation with the formation of intermediates tightly bound on the catalyst surface in the first 7 minutes, while after 2 hours, most of the bound phenoxide has been converted to the product (*i.e.*, cyclohexane), which was readily desorbed from the catalyst surface and swept out of the cell as confirmed by mass spectrometry.

Careful examination of INS spectra of the 1st reacted and adsorbed phenol shows the appearance of new peaks at 197, 314, 486, 655, 784, 857, 896, 1341 and 1452 cm^{-1} as indicated by the up arrow and reduced intensity of INS peaks at 966 and 1167 cm^{-1} as indicated by the down arrow (Fig. 3a). This clearly indicated the formation of new stable substrates bound on the catalyst surface during the reaction. In order to identify the formed species, the spectrum of the 1st reacted phenol on Pd/Nb_2O_5 was compared with that of all possible products (i.e., benzene, cyclohexane, cyclohexene, cyclohexanol and cyclohexanone). It can be seen that eight out of the nine new peaks (marked with green up arrow) show excellent agreement with the spectrum of cyclohexanone (in terms of peak positions), which strongly suggests the formation of cyclohexanone bound on the catalyst surface upon reaction. The comparison of INS spectra for the bound and free cyclohexanone further revealed a number of reductions on peak intensity at 314, 486 and 655 cm^{-1} (assigned to ring-rocking, boat-to-chair conformational and ring-deformational modes, respectively) upon adsorption, consistent with the restricted motion of bound cyclohexanone on the catalyst surface through the C=O end. The remaining new peak at 784 cm^{-1} in the 1st reacted INS spectrum (marked with cyan up arrow) could possibly match with the band at 752 cm^{-1} in the spectrum of cyclohexanone (assigned as the combination of $–CH_2–$ rocking and C6-ring contraction). The small blue shift of this peak is due to (i) the binding interaction between cyclohexanone and the catalyst surface, which induces a stiffening effect of the host-guest system, and (ii) the activation of the C=O bond from adsorbed cyclohexanone molecules, and thus more electrons are donated to the C6-ring. The sharp increase of the bands at 1341 and 1452 cm^{-1} (both assigned as $-CH_2-$ scissoring modes) clearly indicates the hydrogenation of the C6-ring. The decreased bands at 966 and 1167 cm^{-1} on the INS spectrum of the 1st reacted phenol (assigned to the twisting and scissoring modes of the –CH– on the phenol ring, respectively) indicate the reduction of these modes during the formation of cyclohexanone, and imply the retention of strong binding interaction between the phenol ring and the catalyst surface under the HDO conditions. To further consolidate the conclusions, the *in situ* FTIR over Pd/Nb_2O_5 catalysts after phenol adsorption and reaction were also conducted and the results from FTIR were consistent with those from INS (Fig. S19).

The HDO reaction of phenol over the Pt/Nb_2O_5 catalyst was also examined by INS to understand its reaction pathway. Pt/Nb_2O_5 was activated in He and reduced by H_2 in a similar manner as with Pd/Nb_2O_5. Upon reduction, the INS spectrum shows similar features to that of Pd/Nb_2O_5 (Fig. S11). Comparison of the INS spectrum of adsorbed phenol on Pt/Nb_2O_5 with that of the solid phenol confirms several changes (Fig. 3b, S12). The changes for INS peaks at below 120 cm^{-1}, between 155 and 240 cm^{-1}, and at 532, 724, 1226 and 1382 cm^{-1} are similar to those in the case of Pd/Nb_2O_5, indicating that adsorption of phenol occurred primarily at the surface Nb^{5+} sites in both cases and the low loading of noble metal has negligible effect on phenol adsorption. INS spectra of the reaction system were collected after the H_2/phenol stream flowing through the phenol adsorbed catalyst at 150 °C for 7 and 15 minutes (Fig. S13). Little change has been observed in the INS spectrum for the 1st and 2nd reacted phenol, indicating that the bound phenoxide molecules underwent rapid conversion to cyclohexanol, the presence of which was indicated by the very small increases in peak intensity at 856, 1026, 1376 and 1463 cm^{-1}, and subsequently to cyclohexene, benzene and cyclohexane, all with small energy barriers. Benzene and cyclohexane were readily desorbed from the surface and swept out of the cell as confirmed by mass spectrometry. To enrich the formation of possible intermediates on the surface, a 3rd HDO reaction was carried out for 30 minutes under static conditions. The INS spectrum for the 3rd reacted phenol on Pt/Nb_2O_5 matched tightly to that of solid cyclohexane across the whole spectrum with the representative peaks at 243, 388, 425, 521, 784, 858, 906, 1058, 1106, 1273, 1344 and 1442 cm^{-1}. The decreased signal-to-noise ratio is due to the poor adsorption between cyclohexane and the catalyst surface. There is an absence of notable formation of cyclohexanone on Pt/Nb_2O_5 and the rapid conversion of cyclohexanol to cyclohexene, benzene and cyclohexane is highly consistent with the time profile of product distribution shown in Fig. 1c.

Thus, the INS study has confirmed (i) the molecular details of the strong interaction between adsorbed phenol molecules and the catalyst surface (deprotonation to form phenoxide bound on surface Nb^{5+} sites), which is the first essential step for the catalytic transformation to occur; (ii) on the Pd/Nb_2O_5 catalyst, the formation of the cyclohexanone intermediate was evidently observed, suggesting that the hydrogenation of phenyl rings has higher selectivity than the direct cleavage of C–O bonds owing to the strong binding of the phenyl ring to the catalyst surface and high hydrogenation activity of Pd; (iii) on the Pt/Nb_2O_5 catalyst, the HDO reaction undergoes a combination of DDO process and tandem route with fast kinetics, leading to a higher selectivity of arene than that of Pd/Nb_2O_5 at the beginning of the reaction. Overall, this INS study is in excellent agreement with the proposed reaction pathways (Fig. 2) and has provided molecular origins into these important HDO reactions. Interestingly, the mechanisms of HDO of phenol over Pd/Nb_2O_5 and Pt/Nb_2O_5 are distinct from that over Ru/Nb_2O_5, where direct cleavage of C–O bond in phenol is the main process.[5c] Thus, this study confirms that choice of noble metal, albeit at low loading (2% in this case), is directly relevant to the product selectivity in biomass conversion.

4 Conclusions

We have presented the direct HDO of raw lignin into liquid hydrocarbons over the M/Nb_2O_5 (M=Pd, Pt) catalysts, achieving high yields, in particular for the conversion of lignin monomers into C_7-C_9 hydrocarbons. In the HDO process, phenolic intermediates are formed by the cleavage of $C_{aliphatic}$–O ether bonds in lignin, and further converted by hydrogenolysis to hydrocarbons. Model compound studies revealed that the HDO reaction over these two catalysts undergo different pathways. *In situ* INS has been applied to directly visualise the adsorption, binding and conversion of phenol over these two catalysts, providing key molecular insight to their catalytic activity. These emerging niobia-based catalysts have shown strong and specific adsorption of biomass-derived phenolic compounds and thus enabled their efficient catalytic conversion to hydrocarbons as fuels and feedstocks.

Acknowledgements

We thank the National Natural Science Foundation of China (No. 91545103, 21603072, 21832002, 21872050， 21808063), the Fundamental Research Funds for the Central Universities (222201718003, 222201817022), the Science and Technology Commission of Shanghai Municipality (10dz2220500), EPSRC (EP/P011632/1) and the University of Manchester for funding. We especially thank ORNL/SNS and STFC/ISIS for the access to neutron scattering beamlines VISION and TOSCA, respectively. We are also grateful to ORNL and STFC for computing resources.

References

1 (a) A. M. Ruppert, K. Weinberg, and R. Palkovits, *Angew. Chem. Int. Ed.*, 2012, **51**, 2564-2601; (b) Y. Nakagawa, M. Tamura, and K. Tomishige, *ACS Catal.*, 2013, **3**, 2655-2668.

2 P. C. H. Mitchell, *Vibrational spectroscopy with neutrons: with applications in chemistry, biology, materials science and catalysis, Vol. 3*, World Scientific, 2005.

3 (a) C. O. Tuck, E. Pérez, I. T. Horváth, R. A. Sheldon, and M. Poliakoff, *Science*, 2012, **337**, 695-699; (b) J. N. Chheda, G. W. Huber, and J. A. Dumesic, *Angew. Chem. Int. Ed.*, 2007, **46**, 7164-7183; (c) C. Li, M. Zheng, A. Wang and T. Zhang, *Energy Environ. Sci.*, 2012, **5**, 6383-6390; (d) Z. Sun, B. Fridrich, A. Santi, S. Elangovan and K. Barta, *Chem. Rev.* 2018, **118**, 614-678.

4 (a) A. Rahimi, A. Ulbrich, J. J. Coon, and S. S. Stahl, *Nature*, 2014, **515**, 249-252; (b) A. Rahimi, A. Azarpira, H. Kim, J. Ralph, and S. S. Stahl, *J. Am. Chem. Soc.*, 2013, **135**, 6415-6418; (c) T. H. Parsell, B. C. Owen, I. Klein, T. M. Jarrell, C. L. Marcum, L. J. Haupert, L. M. Amundson, H. I. Kenttämaa, F. Ribeiro, J. T. Miller, and M. M. Abu-Omar *Chem. Sci.*, 2013, **4**, 806-813; (d) S. Van den Bosch, W. Schutyser, R. Vanholme, T. Driessen, S. F. Koelewijn, T. Renders, B. De Meester, W. J. J. Huijgen, W. Dehaen, C. M. Courtin, B. Lagrain, W. Boerjan and B. F. Sels, *Energy Environ. Sci*. 2015, **8**, 1748-1763; (e) L. Shuai, M. T. Amiri, Y. M. Questell-Santiago, F. Héroguel, Y. Li, H. Kim, R. Meilan, C. Chapple, J. Ralph, and J. S. Luterbacher, *Science*, 2016, **354**, 329-333; (f) C. F. Zhang, H. J. Li, J. M. Lu, X. C. Zhang, K.E. MacArthur, M. Heggen, and F. Wang, *ACS Catal.* 2017, **7**, 3419-3429; (g) R. Behling, S. Valange, and G. Chatel, *Green Chem.* 2016, **18**, 1839-1854; (h) T. L. Lohr, Z. Li, and T. J. Marks, *ACS Catal.* 2015, **5**, 7004-7007; (i) M. Saidi, F. Samimi, D. Karimipourfard, T. Nimmanwudipong, B. C. Gates, and M. R. Rahimpour, *Energy Environ. Sci.* 2014, **7**, 103-129; (j) T. H. Parsell, B. C. Owen, I. Klein, T. M. Jarrell, C. L. Marcum, L. J. Haupert, L. M. Amundson, H. I. Kenttamaa, F. Ribeiro, J. T. Miller, and M. M. Abu-Omar, *Chem. Sci.* 2013, **4**, 806-813; (k) X. M. Huang, O. M. Morales Gonzales, J. D. Zhu, T. I. Korányi, M. D. Boot, and E. J. M. Hensen, *Green Chem*., 2017, **19**, 175-187; (l) S. Gillet, M. Aguedo, L. Petitjean, A. R. C. Morais, A. M. da Costa Lopes, R. M. Lukasik and P. T. Anastas, *Green Chem.*, 2017, **19**, 4200-4233; (m) C. Li, X. Zhao, A. Wang, G. W. Huber and T. Zhang, *Chem. Rev.,*2015, **115**, 11559−11624.

5 (a) A. Toledano, L. Serrano, A. M. Balu, R. Luque, A. Pineda, and J. Labidi, *ChemSusChem*, 2013, **6**, 529-536; (b) Q. Song, F. Wang, J. Cai, Y. Wang, J. Zhang, W. Yu, and J. Xu, *Energy Environ. Sci.*, 2013, **6**, 994-1007; (c) Y. Shao, Q. N. Xia, L. Dong, X. H. Liu, X. Han, S.F. Parker, Y. Q. Cheng, L. L. Daemen, A. J. Ramirez-Cuesta, S. H. Yang, and Y. Q. Wang, *Nat. Commun*., 2017, **8**, 16104; (d) N. Yan, C. Zhao, P. J. Dyson, C. Wang, L. T. Liu, Y. Kou, ChemSusChem, 2008, **1**, 626-629; (e) W. Schutyser, T. Renders, S. Van den Bosch, S.-F. Koelewijn, G. T. Beckham and B. F. Sels, *Chem. Soc. Rev.*, 2018, **47**, 852-908.

6 (a) D. Y. Hong, S. J. Miller, P. K. Agrawal, and C. W. Jones, *Chem. Commun.*, 2010, **46**, 1038-1040; (b) C. Zhao, Y. Kou, A. A. Lemonidou, X. Li, and J. A. Lercher, *Angew. Chem. Int. Ed.*, 2009, **48**, 3987-3990; (c) Y. Yoon, R. Rousseau, R. S. Weber, D. Mei, and J. A. Lercher, *J. Am. Chem. Soc.*, 2014, **136**, 10287-10298.

7 (a) Z. Luo, Y. Wang, M. He, and C. Zhao, *Green Chem.*, 2016, **18**, 433-441; (b) X. Wang, R. Rinaldi, *Angew. Chem. Int. Ed.*, 2013, **52**, 11499-11503.

8 (a) C. Zhao, D. M. Camaioni, and J. A. Lercher, *J. Catal.*, 2012, **288**, 92-103; (b) C. Zhao, J. He, A. A. Lemonidou, X. Li, and J. A. Lercher, *J. Catal.*, 2011, **280**, 8-16; (c) J. He, C. Zhao, and J. A. Lercher, *J. Catal.*, 2014, **309**, 362-375; (d) C. Chen, G. Chen, F. F. Yang, H. Wang, J. Y. Han, Q. F. Ge, and X. L. Zhu, *Chem. Engineer. Sci*., 2015, **135**, 145-154.

9 (a) M. Badawi, J.-F. Paul, E. Payen, Y. Romero, F. Richard, S. Brunet, A. Popov, E. Kondratieva, J.-P. Gilson, and L. Mariey, *Oil Gas Sci. Technol.*, 2013, **68**, 829-840; (b) E. Furimsky, *Appl. Catal. A*, 2000, **199**, 147-190; (c) J. Filley, and C. Roth, *J. Mol. Catal. A: Chem.*, 1999, **139**, 245-252; (d) E. O. Odebunmi, and D. F. Ollis, *J. Catal.*, 1983, ***80***, 56-64; (e) J. Sun, A. M. Karim, H. Zhang, L. Kovarik, X. S. Li, A. J. Hensley, J.-S. McEwen, and Y. Wang, *J. Catal.*, 2013, **306**, 47-57.

10 L. Nie, P. M. de Souza, F. B. Noronha, W. An, T. Sooknoi, and D. E. Resasco, *J. Mol. Catal. A: Chem.*, 2014, **388**, 47-55.

11 L. Nie, and D. E. Resasco, *J. Catal.*, 2014, **317**, 22-29.

12 (a) A. J. Hensley, Y. Wang, and J.-S. McEwen, *ACS Catal.*, 2014, **5**, 523-536; (b) Q. Tan, G. Wang, L. Nie, A. Dinse, C. Buda, J. Shabaker, and D. E. Resasco, *ACS Catal.*, 2015, **5**, 6271-6283; (c) G. Li, J. Han, H. Wang, X. Zhu, and Q. Ge, *ACS Catal.*, 2015, **5**, 2009-2016.

13 (a) D. Lennon, and S. F. Parker, *Acc. Chem. Res.*, 2014, **47**, 1220-1227; (b) S. F. Parker, D. Lennon, and P. W. Albers, *Appl. Spectrosc.*, 2011, **65**, 1325-1341.

14 Q. Xia, Z. Chen, Y. Shao, X. Gong, H. Wang, X. Liu, S. F. Parker, X. Han, S. Yang, and Y. Wang, *Nat. Commun.*, 2016, **7**, 11162.

15 E. E. Harris, J. D'Ianni, and H. Adkins, *J. Am. Chem. Soc.*, 1938, **60**, 1467-1470.

16 Q. N. Xia, Q. Cuan, X. H. Liu, X. Q. Gong, G. Z. Lu, and Y. Q. Wang, *Angew. Chem. Int. Ed.*, 2014, **53**, 9755-9760.

17 D. Ross, V. Antonov, E. Bokhenkov, A. Kolesnikov, E. Ponyatovsky, J. Tomkinson, *Phys. Rev. B*, 1998, **58**, 2591-2595.

Comparison of Two Multifunctional Catalysts [M/Nb_2O_5 (M=Pd, Pt)] for One-Pot Hydrodeoxygenation of Lignin

Supporting Information

1. Physical characterisation of the catalysts and extracted lignin.

Table S1. GPC analysis of isolated lignin from birch wood.

Sample	M_w (g mol^{-1})	M_n (g mol^{-1})	M_w/M_n
Birch lignin	3214	1700	1.89

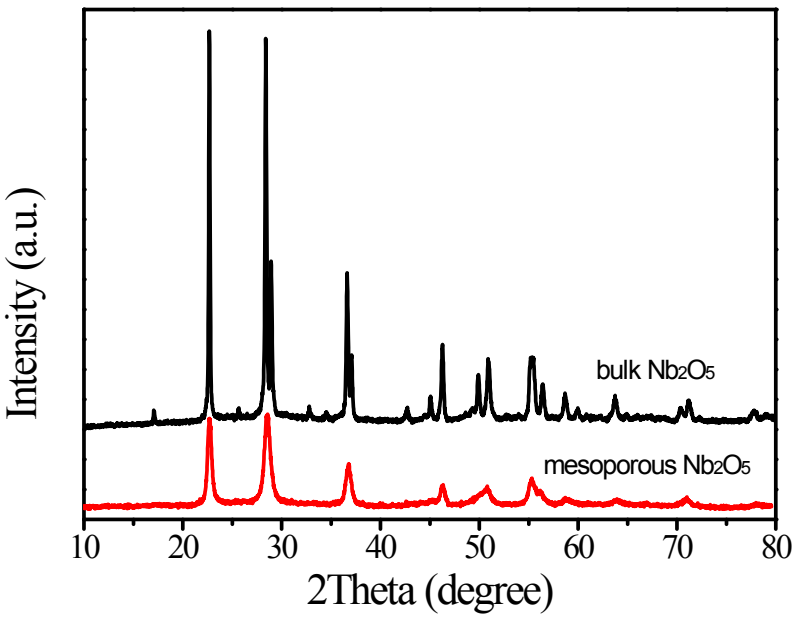

Figure S1. XRD patterns of mesoporous Nb_2O_5 and bulk Nb_2O_5.

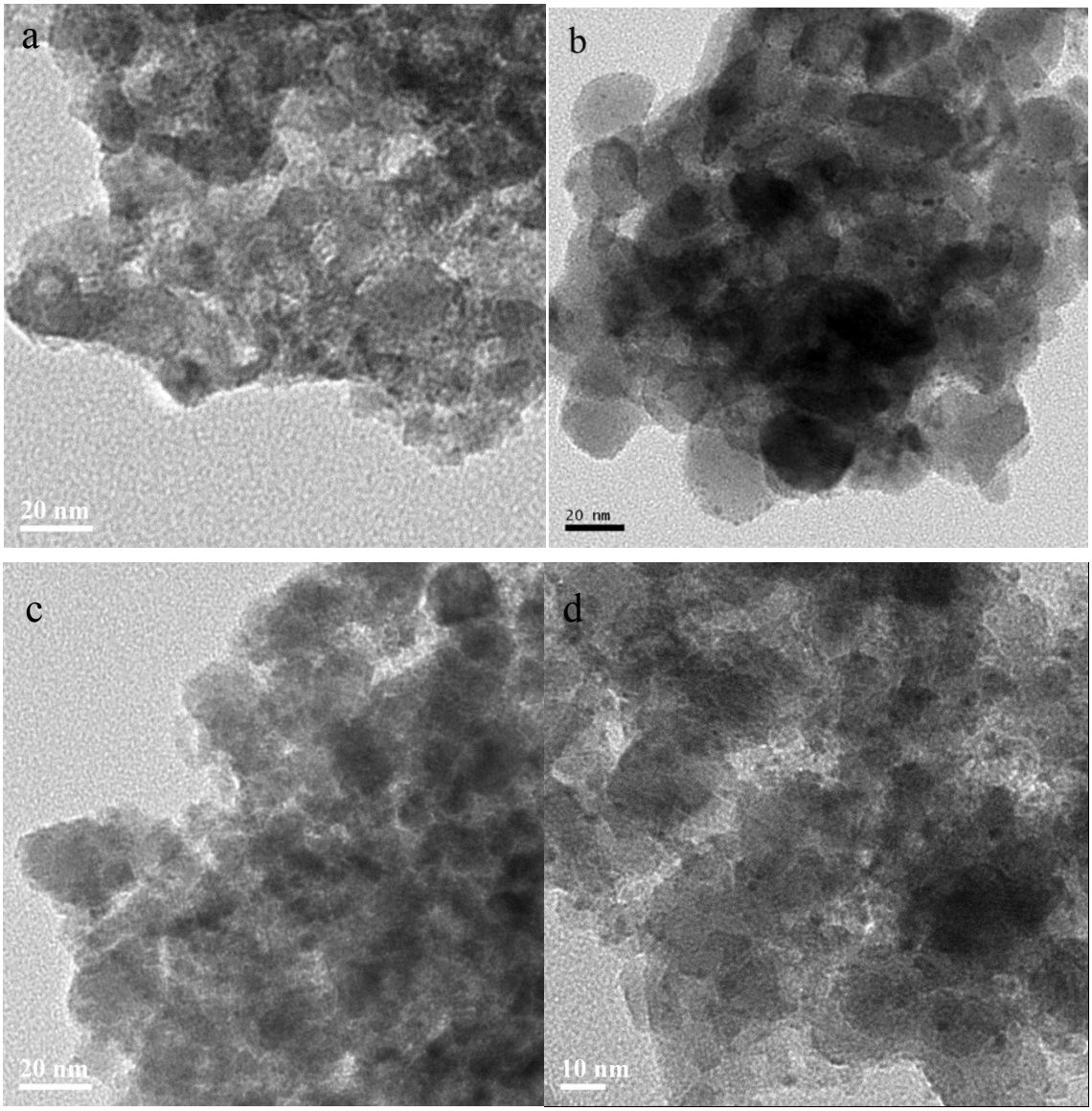

Figure S2. TEM images of fresh catalysts and used catalysts after four recycling runs: (a) Pd/Nb_2O_5, (b) Pt/Nb_2O_5, (c) used Pd/Nb_2O_5 and (d) used Pt/Nb_2O_5.

Table S2. Chemical composition of raw lignin before reaction.

Sample	Element content (wt%)				
	C	H	O	N	S
Birch lignin	64.8	7.3	27.9	0.1	0.0
Alkaline lignin	63.6	6.3	28.1	0.6	1.4

2. Analysis of lignin monomers by alkaline nitrobenzene oxidation method (NBO).

NBO was performed following a reported literature procedure.[3,4] In a typical reaction, extracted birch lignin (40 mg) was mixed with nitrobenzene (0.4 mL) and 2 M NaOH (7 mL) and reacted at 170°C for 2 h in an oil bath. Afterwards, the reactor was cooled in ice-water and 1 mL of freshly prepared ethyl vanillin (3-ethoxy-4-hydroxybenzaldehyde, **EV**) (5 μmol/mL) in 0.1 M NaOH solution was added to the reaction mixture as an internal standard. The mixture was transferred to a 100-mL separation funnel and washed three times with 15 mL of dichloromethane. The remaining aqueous layer was acidified with 2 M HCl, until the pH was below 3.0 and extracted twice with 20 mL of dichloromethane and 20 mL of diethyl ether. The combined organic layer was washed with deionised water (20 mL) and dried over Na_2SO_4. After filtration, the filtrate was collected in a 100-mL pear-shaped flask and dried under reduced pressure. For the TMS (trimethylsilyl) derivatisation step, NBO-products were washed with pyridine (3 × 200 μL) into a GC vial and BSTFA (150 μL) was added. The mixture was heated to 50 °C for 30 min. The silylated NBO-products were analyzed by GC-MS (Agilent 7890A GC-MS) equipped with aHP-5 capillary column (30 m × 250 μm) to identify the products by the comparison with the peak retention time and mass spectra of the authentic compounds. The identified products were quantified by GC-FID (Agilent 7890B) using the same column. Initial column temperature: 150°C (held for 10 min), raised at 5 °C/min to 280 °C (held for 20 min).

In the reported lignin upgrading reaction, the total yields of C_7~C_9 hydrocarbons on Pd/Nb_2O_5 (25.1 wt%, 2020 μmol/g lignin) and Pt/Nb_2O_5 catalysts (28.2 wt%, 2335 μmol/g lignin) were comparable with the yield of 2741 μmol/g lignin obtained through nitrobenzene oxidation (NBO) method (Figure S3), which is an established lignin monomer analysis method. This indicates that the total yields of C_7~C_9 hydrocarbons here is close to the theoretical yield.

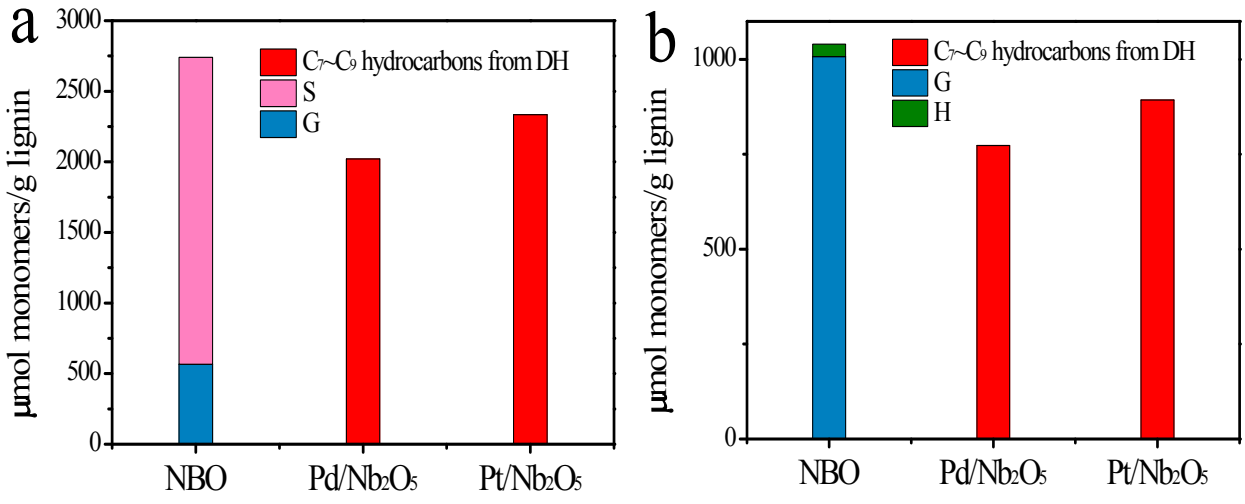

Figure S3. Analysis of (a) birch lignin and (b) alkaline lingnin monomer. "NBO" refers to the nitrobenzene oxidation method; "DH" refers to direct hydrogenolysis; "S" refers to syringy units; "G" refers to guaiacyl units.

3. Stability test

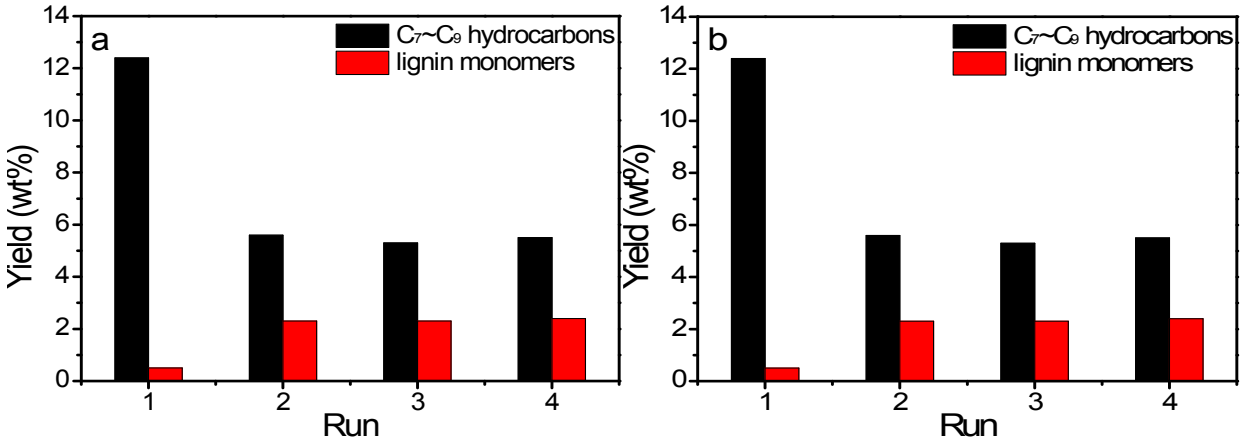

Figure S4 Recycling tests of lignin conversion over (a) Pd/Nb_2O_5 and (b) Pt/Nb_2O_5 catalysts with substrate (0.1 g)/catalyst (0.1 g) ratio. Reaction conditions: lignin 0.1 g, catalyst 0.1 g, 0.1 g, H_2O 15 mL, 250 °C, H_2 0.7 MPa, 20 h, stirring at 1000 rpm.

Table S3. Summary of product distribution from recycling tests of birch lignin conversion over Pd/Nb_2O_5 and Pt/Nb_2O_5.[a]

		Products distribution (wt%)							Total mass Yield (wt%)
		C_7~C_9 arenes			C_7~C_9 cycloalkanes				
Catalyst	Recycling	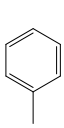	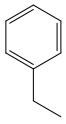	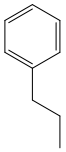	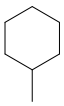	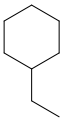	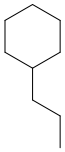	Lignin monomers[b]	
Pd/Nb_2O_5	Run 1	0.0	0.1	0.8	0.1	3.4	8.0	0.5	12.4
Pd/Nb_2O_5	Run 2	0.0	0.1	0.5	0.1	1.9	3.1	2.3	8.0
Pd/Nb_2O_5	Run 3	0.0	0.1	0.4	0.1	1.9	2.9	2.3	7.7
Pd/Nb_2O_5	Run 4	0.0	0.1	0.5	0.1	1.9	2.9	2.4	7.9
Pt/Nb_2O_5	Run 1	0.1	1.4	1.4	0.2	6.1	4.1	0.5	13.8
Pt/Nb_2O_5	Run 2	0.1	0.4	0.4	0.2	3.2	2.1	2.0	8.4
Pt/Nb_2O_5	Run 3	0.1	0.5	0.5	0.3	3.3	2.1	2.1	8.9
Pt/Nb_2O_5	Run 4	0.1	0.4	0.5	0.2	3.1	2.2	1.9	8.4

[a] Reaction conditions: lignin 0.1 g, catalyst 0.1g, H_2O 15 mL, 250 °C, H_2 0.7 MPa, 20h, stirring at 1000 rpm. The metal loading in each catalyst was at 2 wt%.
[b] The lignin monomers contain C_7-C_9 monocyclic oxygenated compounds and hydrocarbons.

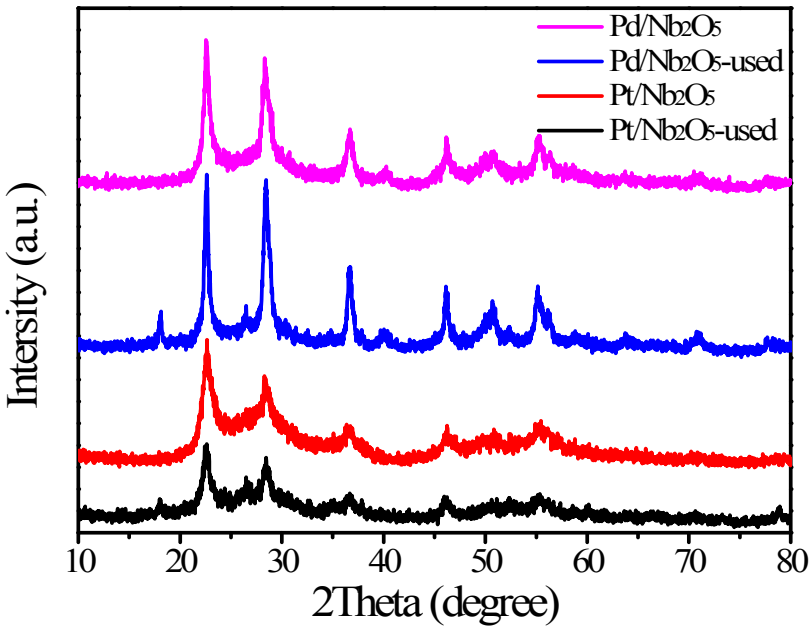

Figure S5. XRD patterns of fresh catalysts and used catalysts after four recycling runs.

4. Additional catalysis data.

Table S4. Summary of product yields from direct hydrodeoxygenation of birch lignin over Pd/Nb_2O_5 and Pt/Nb_2O_5 with different substrate/catalyst ratios.[a]

Catalyst	Amount of catalyst (g)	Products distribution (wt%)									Total mass Yield (wt%)/(C %)
		C_7~C_9 arenes			C_7~C_9 cycloalkanes			Other C_7~C_9[b]	C_{10}~C_{15}[c]	Others[d]	
		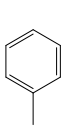	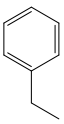	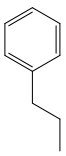	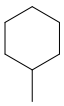	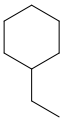	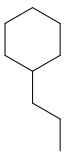				
Pd/Nb_2O_5	0.2g	0.2	0.4	1.7	3.3	7.4	10.4	1.7	3.7	3.1	31.9/42.2
Pd/Nb_2O_5	0.1g	0.0	0.1	0.8	0.1	3.4	8.0	0.1	0.3	0.1	12.9/17.1
Pt/Nb_2O_5	0.2g	0.2	1.5	2.1	1.8	10.4	11.2	1.0	3.0	3.5	34.7/46.1
Pt/Nb_2O_5	0.1g	0.1	1.4	1.4	0.2	6.1	4.1	0.1	0.2	0.2	13.9/18.5

[a] Reaction conditions: lignin 0.1 g, H_2O 15 mL, 250 °C, H_2 0.7 MPa, 20h, stirring at 1000 rpm. The metal loading in each catalyst was at 2 wt%.

b 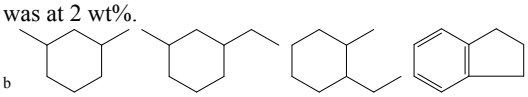

c 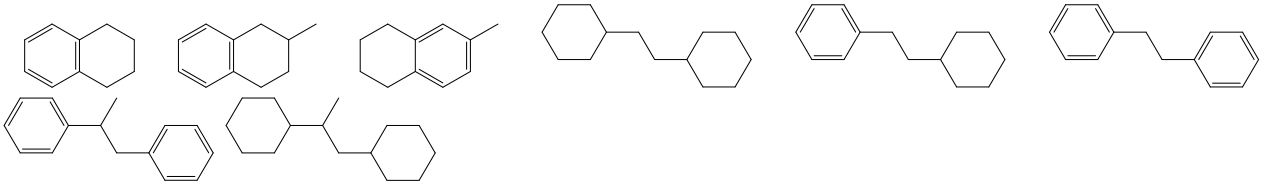

[d] C_{16} and C_{17} aliphatic alkanes and other products were only quantified by GC but not confirmed for structures.

Table S5. Summary of product yields from direct hydrodeoxygenation of alkaline lignin.[a]

Catalyst	Products distribution (wt%)									Total mass Yield (wt%)/(C%)
	C_7~C_9 arenes			C_7~C_9 cycloalkanes			Other C_7~C_9[b]	C_{10}~C_{15}[c]	Others[d]	
	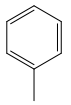	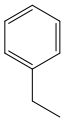	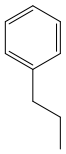	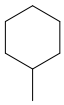	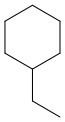	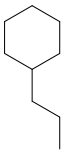				
Pd/Nb_2O_5	0.1	0.2	0.7	1.1	2.7	4.2	0.5	1.5	1.1	12.1/16.3
Pt/Nb_2O_5	0.1	0.5	0.9	0.6	4.2	4.1	0.3	1.1	1.2	13.0/17.6

[a] Reaction conditions: lignin 0.1 g, catalyst 0.2 g, H_2O 15 mL, 250 °C, H_2 0.7 MPa, 20h, stirring at 1000 rpm. The metal loading in each catalyst was at 2 wt%.

b 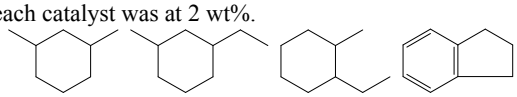

c 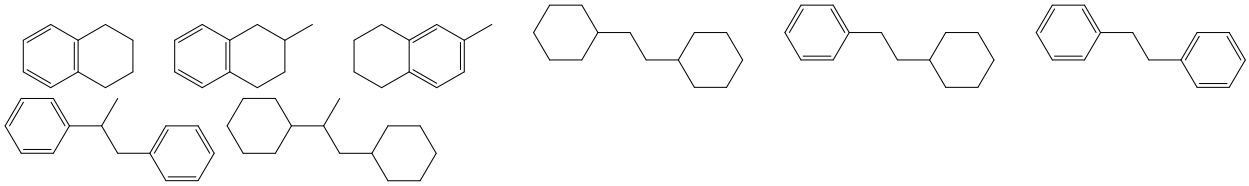

[d] C_{16} and C_{17} aliphatic alkanes and other products were only quantified by GC but not confirmed for structures.

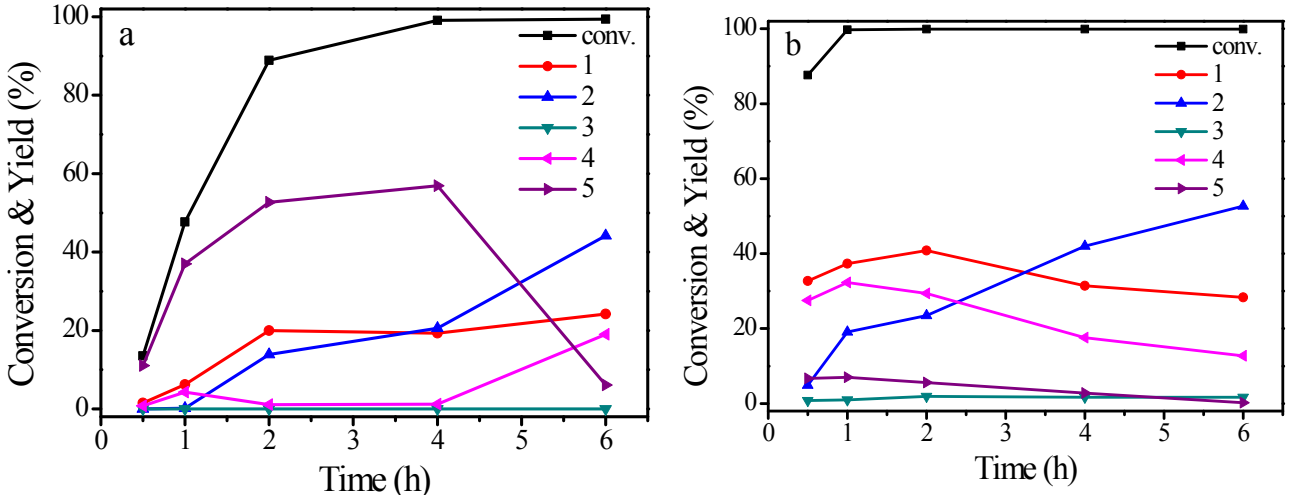

Figure S6. Products distribution for the conversion of 4-methylphenol over Pd/Nb_2O_5 (a) and Pt/Nb_2O_5 (b) catalysts as a function of time. Reaction conditions: substrate 0.2 g, catalyst 0.4 g, H_2O 15 mL, 250 °C, H_2 0.5 MPa, stirring at 1000 rpm.

5. *In situ* inelastic neutron scattering (INS) and DFT calculations

INS spectra were recorded on the TOSCA spectrometer at the ISIS Facility at the STFC Rutherford Appleton Laboratory (UK) and on the VISION spectrometer at Spallation Neutron Source, Oak Ridge National Laboratory (USA). Both TOSCA and VISION are indirect geometry crystal analyser instruments that provide a wide dynamic range (16–4000 cm^{-1}) with resolution optimised in the 50–2000 cm^{-1} range. In this region TOSCA has a resolution of 1.25% of the energy transfer. All the INS spectra for the catalysis system were collected after the sample was cooled and stabilised at temperatures below 30 K.

Approximately 20 g of each catalyst was loaded into a flow type stainless steel cell. By heating at 300 °C under He flow for 3 hours, the trace amount of water that was adsorbed on the catalyst surface was removed. The activated catalyst was then reduced by heating under a H_2 flow at 150 °C for 3 hours. To study the reaction mechanism, phenol was used as a model compound and dosed into the sample cell by a He flow at 150 °C for 3 hours. This allowed the phenol to be adsorbed on the catalyst surface and the INS spectrum of the phenol adsorbed catalyst was collected after cooling to below 30 K. After the data collection, phenol/H_2 was introduced to the cell for 7 min at 150 °C for the catalytic reaction to occur. The exhaust gas was monitored continuously *via* mass spectrometry. A further reaction was carried out by feeding H_2 for an additional 0.5-2 hours at 150 °C. INS spectra of pure solid compounds for both starting material and reaction products were collected at 10 K. A flow chart experimental procedure for the INS experiment was been shown in Fig. S18.

DFT Simulation. DFT calculations of the INS spectra for solid phenol, benzene, cyclohexane, cyclohexanone and cyclohexanol were carried out using their corresponding crystal structures,[5] which can be directly related to the experimental INS spectra of the solid state compounds with no approximations other than the use of DFT eigenvectors and eigenvalues to determine the spectral intensities. The information was used to identify the modes of vibrational features in the experimental INS spectra. No abscissa scale factor was used throughout this report for INS calculations. The calculated INS spectrum shows the total transitions (up to 10 orders). The calculations used the Projector Augmented Wave (PAW) method[6,7] to describe the effects of core electrons, and the Perdew-Burke-Ernzerhof (PBE)[8] implementation of the Generalized Gradient Approximation (GGA) for the exchange-correlation functional. The energy cutoff for the plane-waves is 500 eV, the energy tolerance for electronic structure calculation is 10^{-4} eV, and the maximum force is below 0.01 eV/Å after structural relaxation.

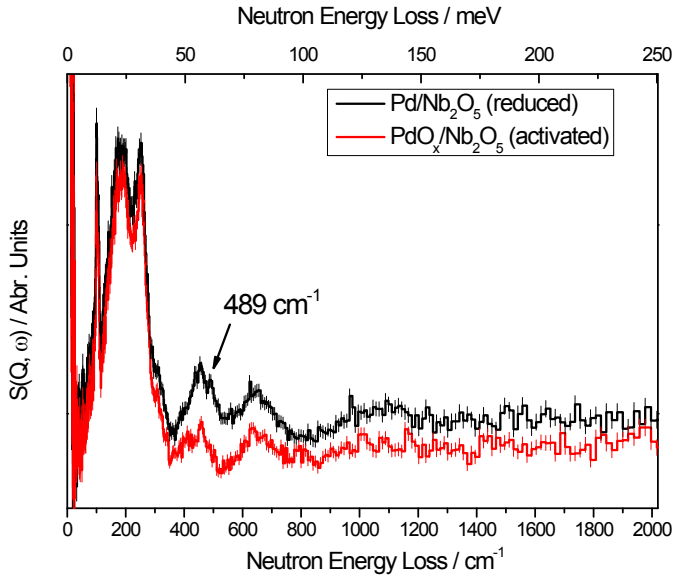

Figure S7. Comparison of INS spectra of the activated and reduced Pd/Nb_2O_5 catalyst.

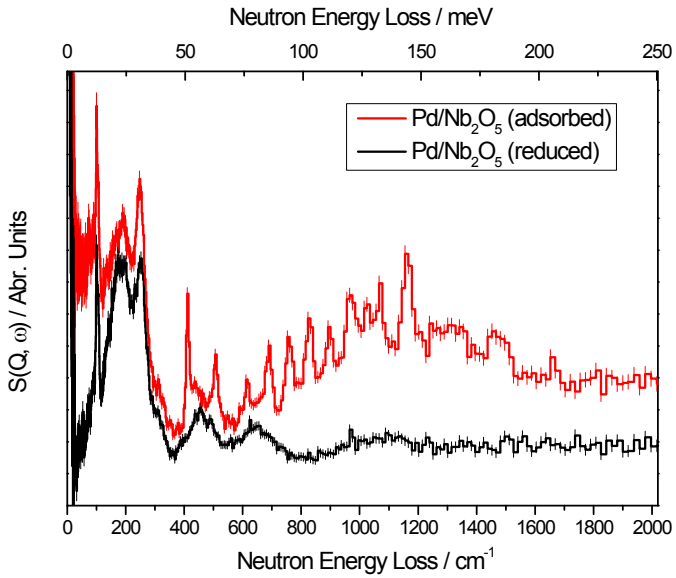

Figure S8. Comparison of the experimental INS spectra for bare Pd/Nb_2O_5 catalyst and the phenol adsorbed catalyst.

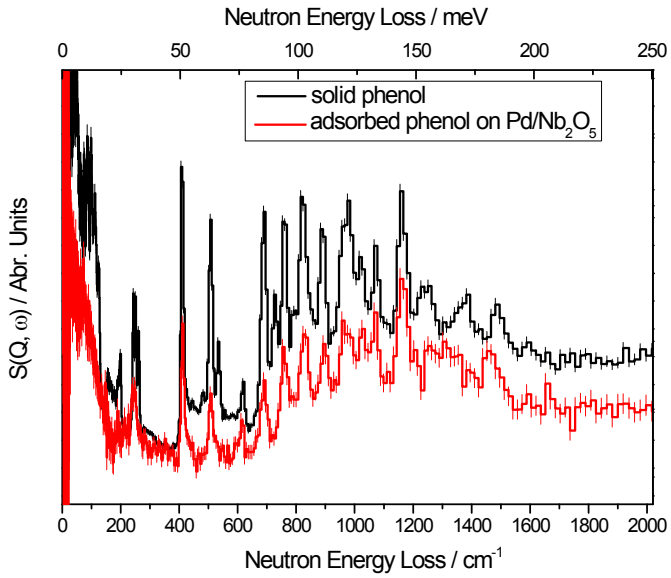

Figure S9. Comparison of the INS spectra of solid phenol and the phenol adsorbed on the Pd/Nb_2O_5 catalyst (obtained by subtracting INS spectrum of the reduced catalyst from the phenol adsorbed catalyst).

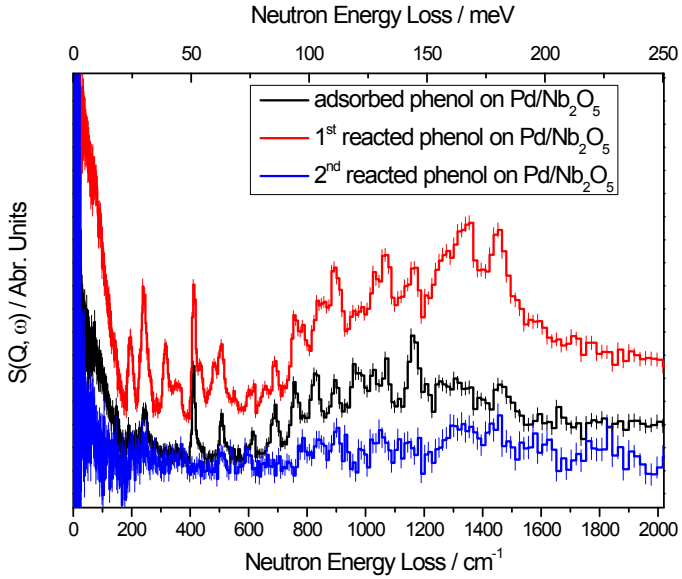

Figure S10. Comparison of INS spectra of the adsorbed, 1st and 2nd reacted phenol on the Pd/Nb_2O_5 catalyst.

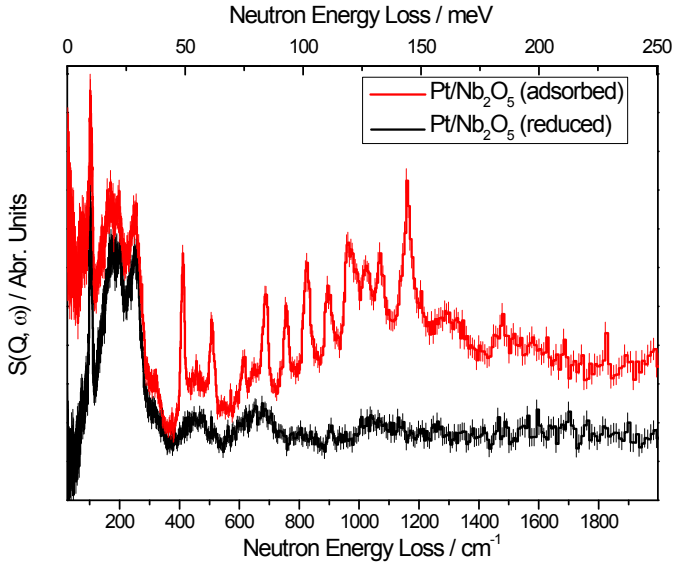

Figure S11. Comparison of the experimental INS spectra for bare Pt/Nb_2O_5 catalyst and the phenol adsorbed catalyst.

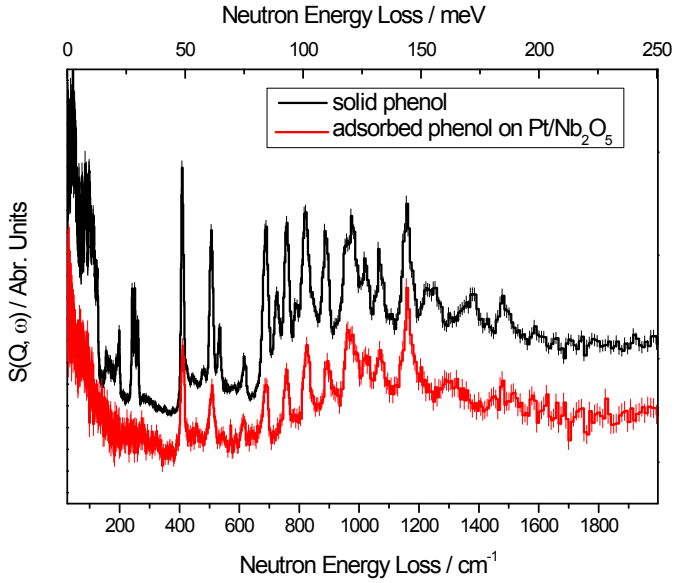

Figure S12. Comparison of the INS spectra of solid phenol and the phenol adsorbed on the Pt/Nb_2O_5 catalyst (obtained by subtracting INS spectrum of the reduced catalyst from the phenol adsorbed catalyst).

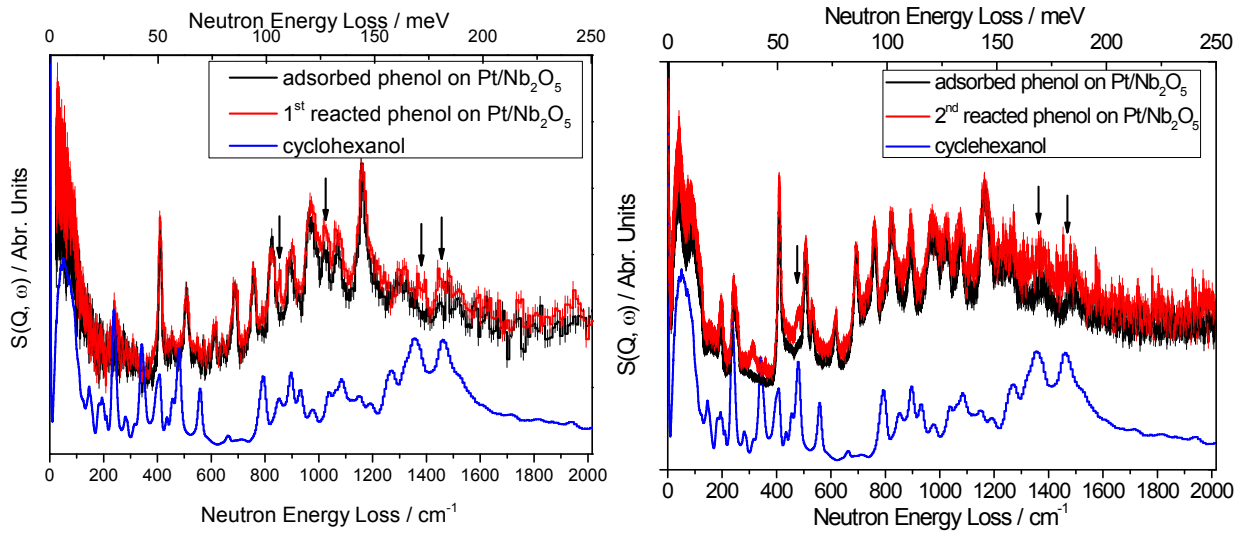

Figure S13. Comparison of INS spectra of the adsorbed and 1st (a) and 2nd (b) reacted phenol on the Pt/Nb_2O_5 catalyst. INS spectrum of solid cyclohexanol is shown for reference. The black arrows indicate the increase of INS features that correlate with the formation of a small amount of cyclohexanol on the catalyst surface.

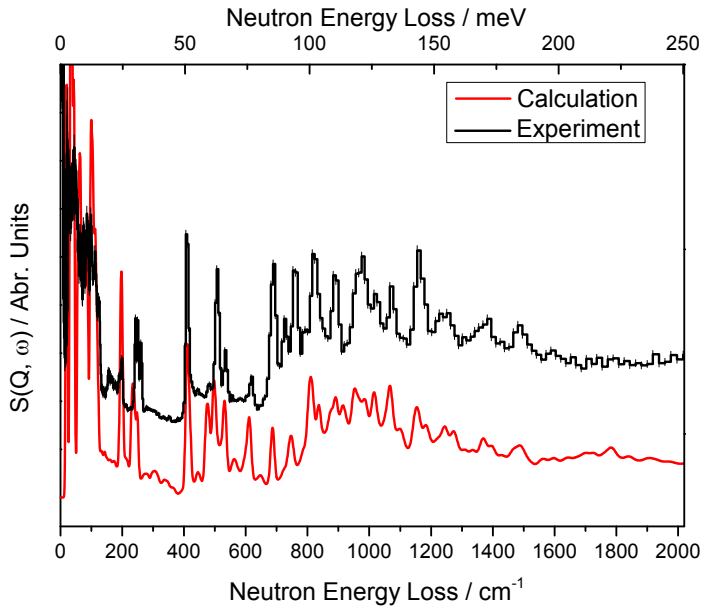

Figure S14. Comparison of calculated and experimental INS spectra of condensed phenol in solid at 10K.

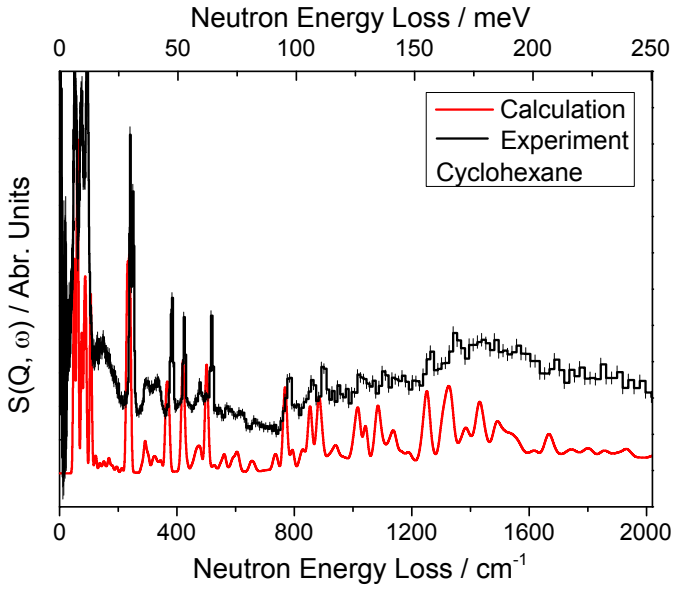

Figure S15. Comparison of calculated and experimental INS spectra of condensed cyclohexane in solid at 10K.

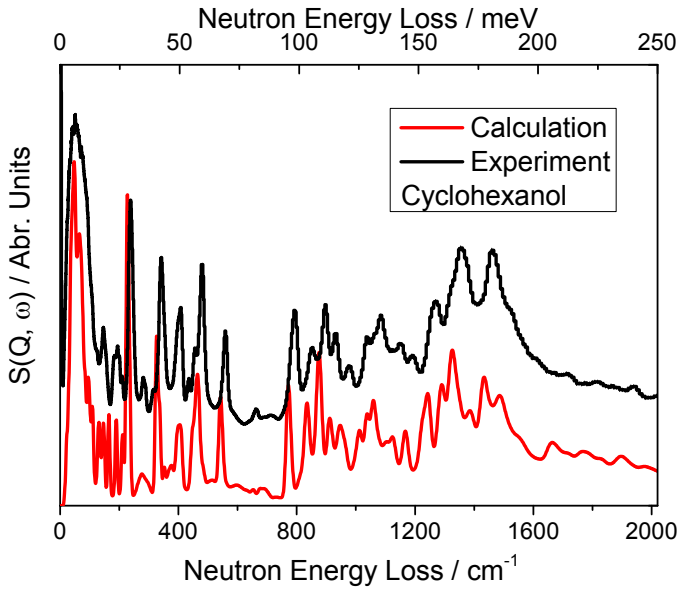

Figure S16. Comparison of calculated and experimental INS spectra of condensed cyclohexanol in solid at 10K.

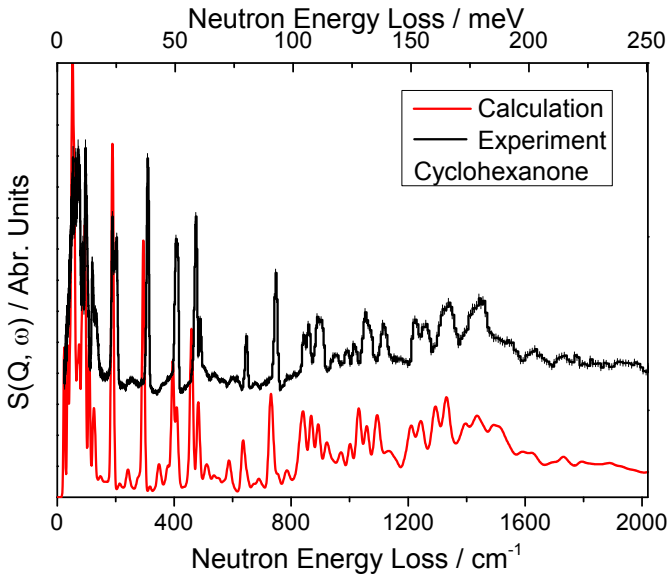

Figure S17. Comparison of calculated and experimental INS spectra of condensed cyclohexanone in solid at 10K.

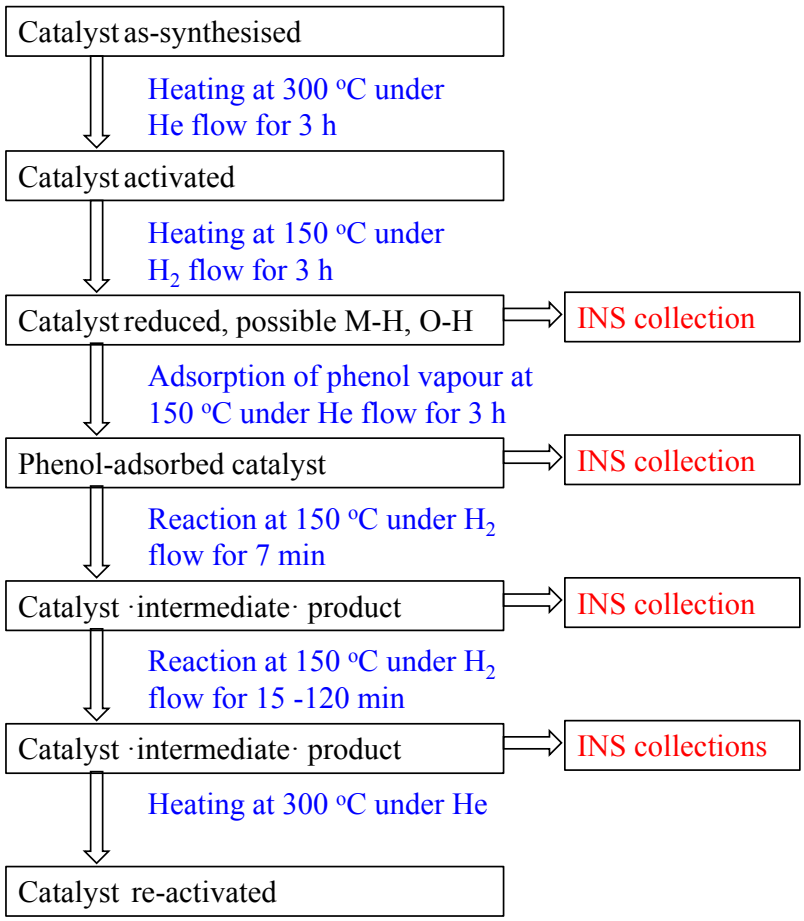

Figure S18. View of a flowchat for the *in situ* INS experiment. Two HDO reactions were carried out for phenol-adsorbed Pd/Nb_2O_5 at the time of 7 and 120 min. Three HDO reactions were conducted for phenol-adsorbed Pt/Nb_2O_5 at the time of 7, 15 and 120 min.

6. *In situ* Fourier Transform infrared spectroscopy (FTIR)

To further consolidate the conclusions, the in situ FTIR over Pd/Nb_2O_5 catalysts after phenol adsorption and reaction were also conducted (Fig. S19). Upon phenol adsorption at 150 °C, the appearance of many new spectral features were observed (3068、3035、1589、1490 and 1267 cm^{-1}), clearly demonstrating the binding of phenol molecules onto the catalyst surface. By comparing the difference spectrum and the FTIR spectra of gas-phase phenol (Fig. S20), a few changes were clearly observed. The intensity of the peak 1333cm^{-1} (assigned to vibration of the δ (OH)) was completely disappeared and the intensity of the peak 1267 cm^{-1} (assigned to vibration of the ν (CO) on phenoxide) was increased, suggesting that deprotonation of adsorbed phenol molecules to form phenoxide bound on the catalyst surface. The peaks at 1589 and 1490 cm^{-1} (assigned to the vibration of the ν ($C=C_{ring}$) on benzene ring) also concurrently shifted, suggesting that the adsorbed phenol molecules are disordered over the catalyst surface and have restricted translational motion owing to the strong binding to the catalyst. The FTIR spectra of the reaction system were collected after an phenol/H_2 stream flowing through the phenol adsorbed catalyst at 150 °C for 5 minutes, 10 minutes and 30 mimnutes. The intensity of the peaks at 1267 cm^{-1} was greatly decreased, while a new peak at 1670 cm^{-1} (assigned to the stretching vibration of the ν (C=O)) was formed. This observation indicates that the adsorbed phenol molecules underwent a 4-methylcyclohexanone as intermediate products and further conversion to produce 4-methylcyclohexanol and methylcyclohexane.

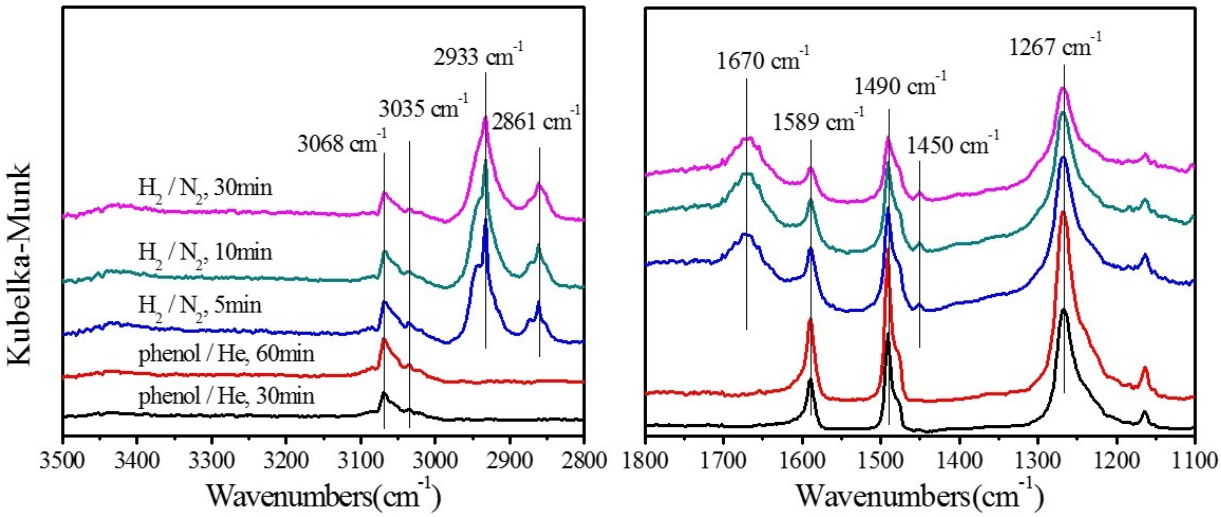

Figure S19. DRIFTS spectra obtained over Pd/Nb_2O_5 catalysts after phenol adsorption for 30 min and 60 min in a phenol/He flow, followed by purge with a 10%H_2/N_2 mixed gas for 5 min, 10 min and 30 min at 150 °C.

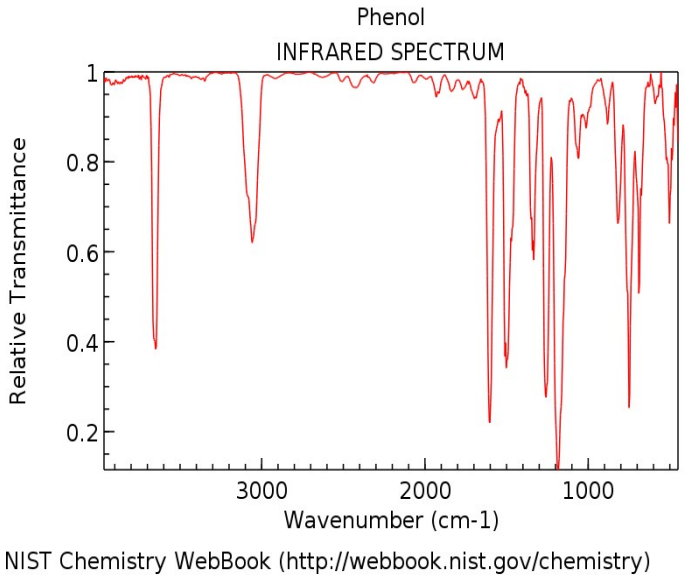

Figure S20. FTIR spectra of gas-phase phenol from NIST Chemistry WebBook.

7. References

[1] Harris, E. E., D'Ianni, J. & Adkins, H. Reaction of hardwood lignin with hydrogen. *J. Am. Chem. Soc.* **60**, 1467-1470 (1938).

[2] Xia, Q. N., Cuan, Q., Liu, X. H., Gong, X. Q., Lu, G. Z., & Wang, Y. Q. Pd/$NbOPO_4$ multifunctional catalyst for the direct production of liquid alkanes from aldol adducts of furans. *Angew. Chem. Int. Ed.* **53**, 9755-9760 (2014).

[3] Shuai, L., Amiri, M. T., Questell-Santiago, Y. M, Héroguel, F., Li, Y., Kim, H., Meilan, R., Chapple, C., Ralph, J. Luterbacher, Jeremy S Formaldehyde stabilization facilitates lignin monomer production during biomass depolymerization. *Science* **354**, 329-333 (2016).

[4] Li, Y., Akiyama, T., Yokoyama, T. & Matsumoto, Y. NMR assignment for diaryl ether structures (4–O–5 structures) in pine wood lignin. *Biomacromolecules* **17**, 1921-1929 (2016).

[5] Kresse, G. and Furthmüller, J. Efficient iterative schemes for *ab initio* total-energy calculations using a plane-wave basis set. *Phys. Rev. B*, 54:11169 (1996).

[6] Blochl, P. E. Projector augmented-wave method. *Phys. Rev. B*, 50:17953 (1994).

[7] Kresse, G. and Joubert, D. From ultrasoft pseudopotentials to the projector augmented-wave method. *Phys. Rev. B*, 59:1758 (1999).

[8] Perdew, J. P., Burke K. and Ernzerhof, M. Generalized gradient approximation made simple. *Phys. Rev. Lett.*, **77**, 3865-3868 (1996).